Preparation, Characterization, and Application of Thin Film Composite Nanofiltration Membranes

Yujun Song,[1]* Fuan Liu,[2] Benhui Sun[1]

[1]*College of Materials Science and Engineering, Beijing University of Chemical Technology, Beijing 100029, China*
[2]*China Textile Academy, Beijing 100025, China*

Received 22 January 2004; accepted 29 July 2004
DOI 10.1002/app.21338
Published online 19 January 2005 in Wiley InterScience (www.interscience.wiley.com).

ABSTRACT: The active aromatic polyamide layers of thin film composite nanofiltration (NF-TFC) membranes were prepared via interfacial polymerization (IP) from three different types of polyamine: *p*-phenylenediamine (PPD), *m*-phenylenediamine (MPD), or piperazine (PRP), and trimesoyl chloride (TMC) on polysulfone/sulfonated polysulfone (PSf/SPSf) alloy substrates. Chemical components, cross section structures, and thermal properties of the polyamide active layers and the bulk membranes, characterized by Fourier transfer IR spectroscopy and attenuated total reflection IR spectroscopy, scanning electron microscopy, and differential scanning calorimetry and thermogravimetry, respectively, revealed an interpenetrating layer between the polyamide active layer and the substrate. A ridge–valley structural active layer was formed on the PSf/SPSf substrate for the NF-TFC membrane with a thick polyacrylamide (PA) layer. Compared with the NF-TFC membranes on PSf substrates, those on PSf/SPSf alloy substrates had a higher permeability without losing the selectivity by introducing the hydrophilic SPSf into the hydrophobic PSf substrates. The binding between the modified substrate and the active PA layer was also improved. Good separation performances using these NF-TFC membranes were obtained in the polyvalent ion separation, the ground water softening, and the treatment of wastewater from adipic acid plants in a wide pH range. © 2005 Wiley Periodicals, Inc. J Appl Polym Sci 95: 1251–1261, 2005

Key words: nanofiltration membrane; separation techniques; thin film composite; polyamides; alloys

INTRODUCTION

Thin film composite nanofiltration (NF-TFC) membranes are novel liquid separation membranes with commercial prospects owing to their high selectivity and permeability under ultralow pressure.[1] These membranes can be applied to separate polyvalent ions and chemicals with molecular weights from 100 to 1,000.[1,2] Both chemical compositions and structures of the active skin and the substrate are crucial for preparing NF-TFC membranes with reasonable cross section structures and excellent separation performance.[3,4] Typically, a polyamide (PA) active layer is formed via interfacial polymerization on a porous substrate, which is usually made of polysulfone (PSf) with a sponge-like porous structure.[1,4] However, the hydrophobic polysulfone and the sponge-like porous substrate (usually having a thick dense top skin) do not favor a further increase of the permeability of the NF-TFC membrane. Strong binding between the hydrophobic polysulfone and the active PA layer is still not a trivial problem for the long-term stable run NF-TFC membrane, although the formation of an interpenetrating layer is suggested between the substrate and the active layer to strengthen the binding.[1,5] In addition, many methods have been developed to characterize the chemical composition of the active layer, while much less has been done about the chemical composition difference between the active skin and the whole membrane to reveal the interpenetrating layer.[6]

In this paper, not only the hydrophilic property and the binding could be improved by introducing sulfonated polysulfone (SPSf) into the porous PSf substrate, but also the asymmetric structure was modified. High-performance NF-TFC membranes were prepared using the modified alloy substrate. Fourier transfer IR spectroscopy (FT-IR) and attenuated total reflection IR spectroscopy (ATR-IR) were used to characterize the chemical composition of the active layer and the bulk membrane. The cross section structures of the NF-TFC membranes were characterized by scanning electron microscopy (SEM). Differential scanning calorimetry (DSC) and thermogravimetry (TGA) were used to investigate the thermal properties of the NF-TFC membranes. All of them were also used to analyze the interpenetrating layer between the substrate and the active PA layer. The separation performance of these membranes was tested by the experiments on polyva-

Correspondence to: Y. Song (ysong2@lsu.edu).
**Present address:* Center for Advanced Micro Structures and Devices of Louisiana State University, 6980 Jefferson Highway, Baton Rouge, LA 70806.

lent ion separation, softening of ground water in Beijing, and treatment of apidic acid wastewater containing high concentrations of nitrides and ammonium salts.

EXPERIMENTAL

Membrane preparation

The PSf/SPSf substrates were prepared by the L-S phase inversion method.[1,5,7] 17% (w/v) of PSf [η = 0.37–0.39 dL/g; 0.2% w/v in CH_3Cl, M_n = 16,000 (MO), Aldrich Chem.] and SPSf (self-made with IEC = 0.65 mEq/g, TsingHua University) with a certain ratio (5–25 wt % SPSf) were dissolved into *N*,*N*′-dimethyformamide (AR, Shiying Chemical Plant, Beijing) with 5 wt % PVP (AR, Xinning Chemical Co., Guangzhou, China) to form the casting solution. The casting solution was then filtered, placed overnight at 45°C in the oven, and then cooled to room temperature to remove bubbles, and then flow-coated on a flat glass plate with uniform thickness to form a liquid film. The liquid film was then immersed into distilled (DI) water to form the solid porous substrate with thickness of 100–220 μm after the solvent was evaporated for 5–180 s.

The active skins were prepared by interfacial polymerization.[3,5,8] Polyamine (PPD; *p*-phenylenediamine, 95%, CP, Wulian Chemical Plant, China), MPD (*m*-phenylenediamine, 98%, Aldrich Chem.), or PRP (piperazine, AR, Shanghai Chemical Reagent Company), surfactant (SBDS, dodecylbenzenesulfonic acid, sodium salt, AR, Beijing Chemical Reagent Company), and phase transfer catalyst were dissolved into DI water to form the reaction solution A. A certain amount of trimesoy chloride (TMC, 99%, Aldrich Chemical Inc.) was dissolved into hexane (99%, AR, XinChun Chemical Reagent Plant, China) to form the reaction solution B. The PSf/SPSf alloy substrate (ϕ5–8 cm) was immersed into solution A for 2–5 min. The substrate was then taken out and placed vertically for 1–2 min, until no water droplets dropped down. Next, the porous alloy substrate was immersed quickly and smoothly into solution B. The membrane was then taken out and air dried after the IP reaction occurred on the porous alloy substrate in solution B for 3–180 s. The dry membrane was then put into the oven at 50–80°C for 5–20 min, or placed at room temperature overnight or longer. After that, the membrane was extracted using 30–40°C DI water for 1–2 h. The NF-TFC membrane was then kept in the DI water for future membrane performance tests.

Membrane structure characterization

FT-IR and ATR-IR (Nicollet IMPACT 400D, Nicollet Inc.) were used to characterize the chemical composition difference between the whole composite membrane and the active layer of the NF-TFC membrane. SEM (S-250, Cambridge; S-450, HITACHI) was used to characterize the cross section of the membrane. The thermal properties of different kinds of membranes were investigated using DSC (Perkin–Elmer TGS-2) and TGA (SDT2960 TA Instruments Inc.) under nitrogen flow at heating ramp of 10 K/min.

Membrane performance characterization

The membrane performance was investigated by a static sealed ultrafiltration chamber with filtration area of 0.002 m^2 under operation pressure change of 0.3 MPa. The selectivity of NF-TFC membranes (*R* %) was calculated using the conductivity differences between the feed solution and the product solution with the total flux of 0.0075 L [eq. (1)]. The permeability (*F*, L m^{-2}·h^{-1}) was calculated from the flux at a unit time on a unit membrane area [eq. (2)].

$$R(\%) = \left(1 - \frac{\lambda_p}{\lambda_f}\right) \times 100 \quad (1)$$

where λ_P is the conductivity of the product ($m\Omega^{-1}$·cm^{-1}) and λ_f is the conductivity of the feed ($m\Omega^{-1}$·cm^{-1}).

$$F = Q/(S \times t) \quad (2)$$

where *Q* is the total volume of the permeated product (L); *S* is the effective membrane area (m^2); and *t* is the time to obtain *Q* liter product (h).

RESULTS AND DISCUSSION

Membrane characterization

Figure 1 shows the FT-IR spectra of the NF-TFC membranes prepared from polyamines (PPD, MPD, or PRP) and TMC on PSf/SPSf alloy substrates. Compared with the standard IR spectrum of Udel polysulfone P-1700,[9,10] it was noted that peaks at 3164.90–3037.64 cm^{-1}, peaks at 2964.58 and 2872.59 cm^{-1}, and peaks at 2925.66 and 2870.10 cm^{-1}, represented the hydrogen group, methyl groups and methane group in the phenyl group of polysulfone, respectively. Not only the characteristic peaks for polysulfone, the asymmetric stretching vibration (γ_{as}) at 1324.52 cm^{-1}, the symmetric stretching vibration (γ_s) at 1149.79 cm^{-1}, and the bending vibration (δ_{SO2}) at 562.72 cm^{-1},[9,11,12] showed in all three samples, but also characteristic peaks for the sulfonic acid group (the symmetric stretching vibration (γ_s) at 2353.66 $cm^{-1}$and the asymmetric stretching vibration (γ_{as}) at 1047.56 cm^{-1})[9] appeared. The wide peak at around 3430 cm^{-1} indicated the stretching vibration of the N–H bond. Peaks

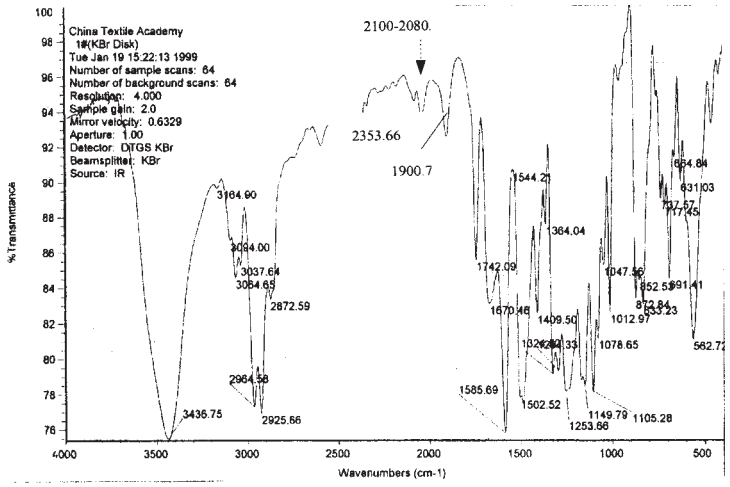

(a) Prepared from PRP and TMC

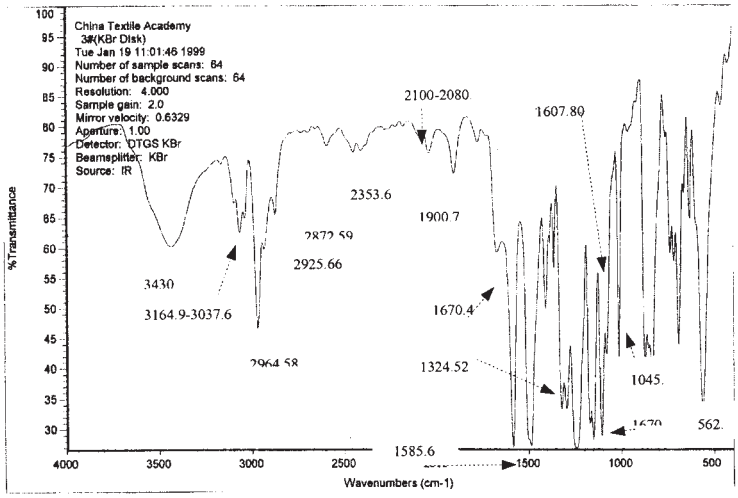

(b) Prepared from MPD and TMC

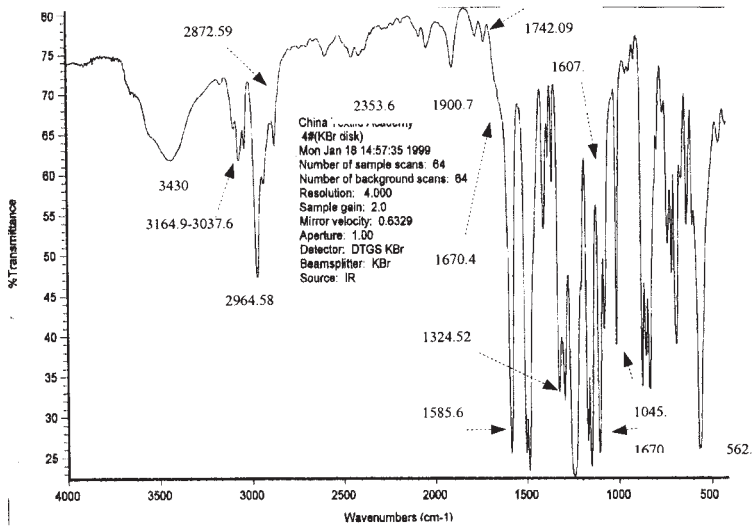

(c) Prepared from PPD and TMC

Figure 1 FT-IR spectra for the bulk NF-TFC membranes on PSf/SPSf substrate.

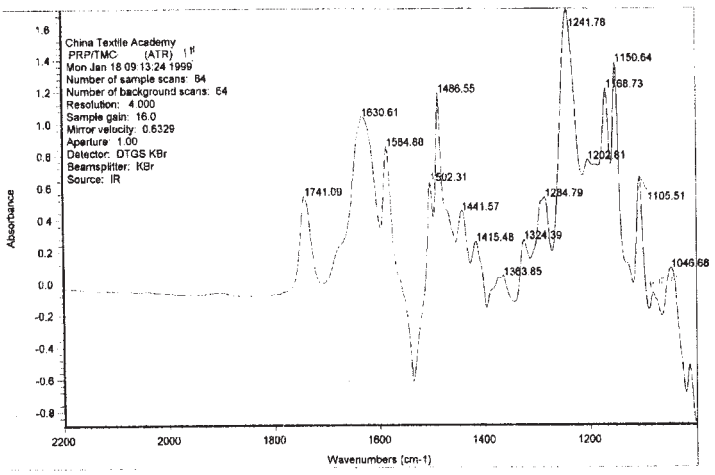

(a) Prepared from PRP and TMC

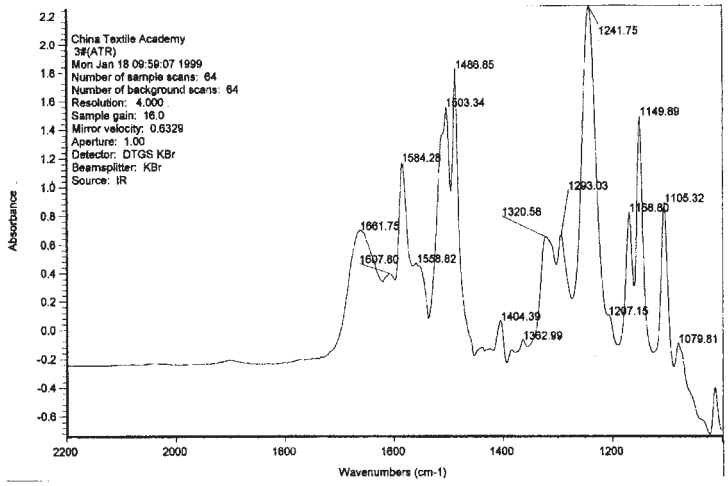

b) Prepared from MPD and TMC

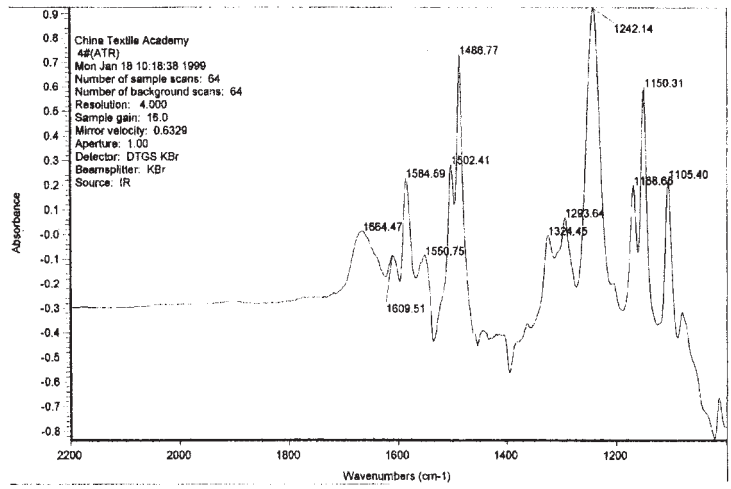

c) Prepared from PPD and TMC

Figure 2 ATR-IR spectra for the surface active layer of NF-TFC membranes.

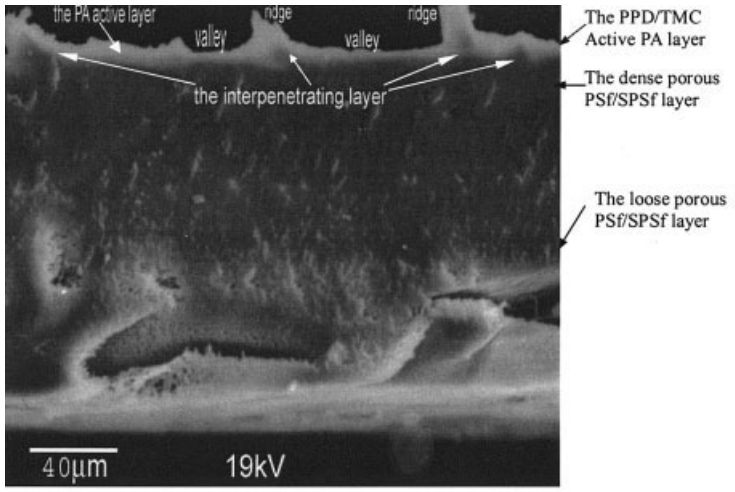

(a) Membrane prepared from PPD/TMC on PSf/SPSf substrate

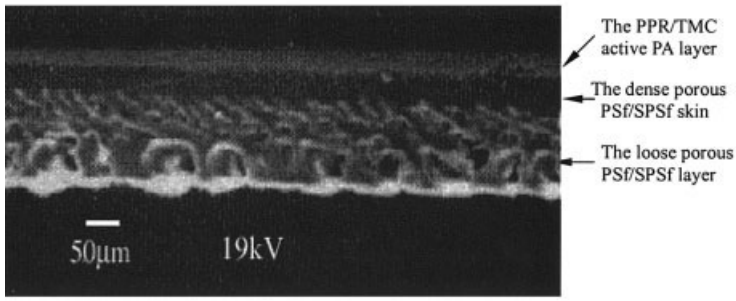

(b) Membrane prepared from PRP/TMC on PSf/SPSf substrate

Figure 3 SEM images of cross section structures for NF-TFC membranes with thick active PA layer.

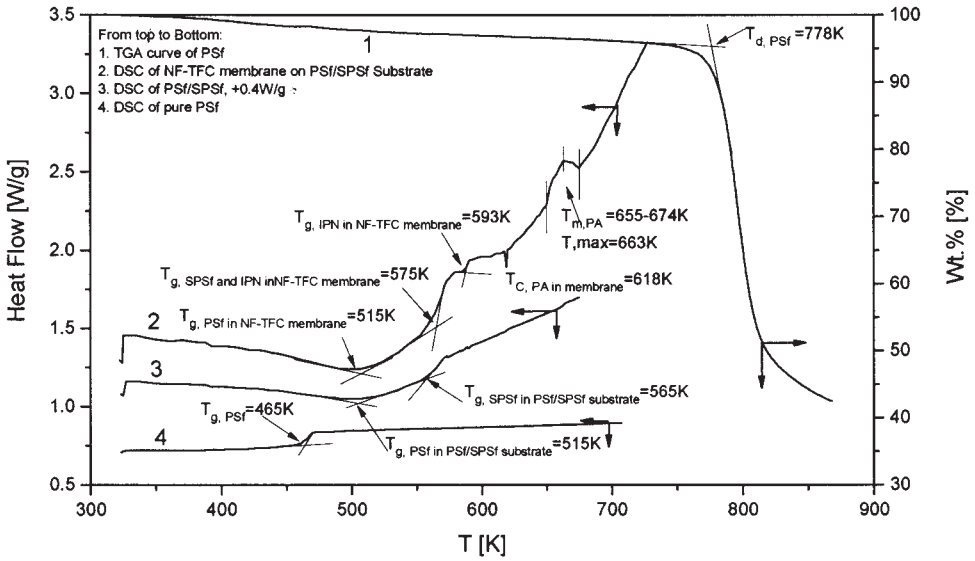

Figure 4 DSC spectra for PSf, PSf/SPSf porous substrates, and NF-TFC membrane prepared from PPD and TMC on PSf/SPSf substrate, and the TGA curve for PSf.

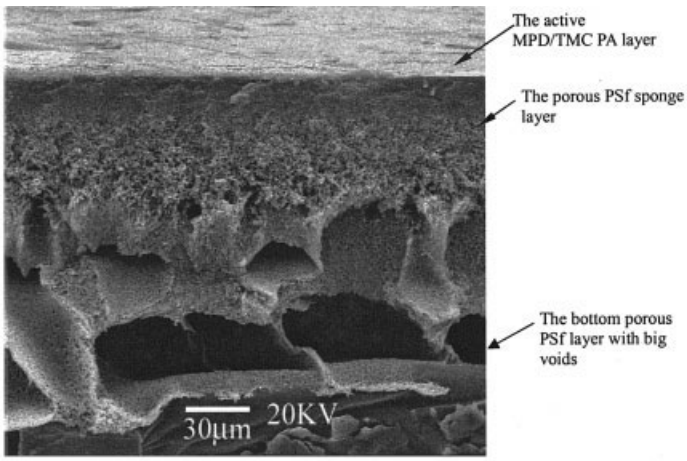

(a) The cross-section of NF-TFC membrane from MPD and TMC on PSf substrate

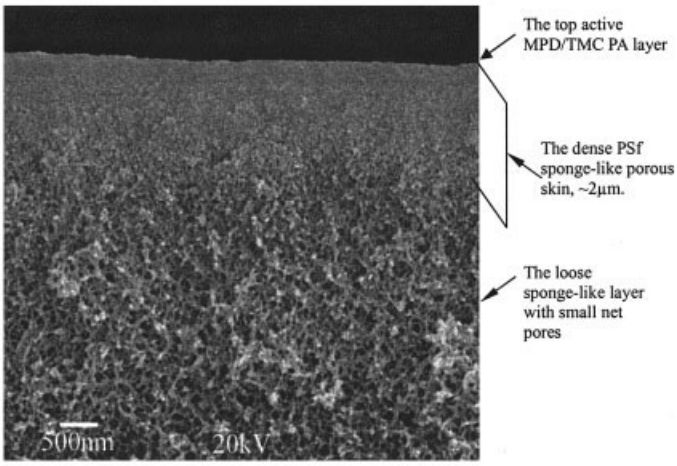

(b) the top active polyamide layer and the porous medium layer of the PSf substrate showi
a thick dense top layer.

Figure 5 SEM images of cross section structures of NF-TFC membrane prepared on PSf substrate.

at 1670.46 cm^{-1} in Figure 1(a), 1670.47 cm^{-1} in Figure 1(b), and 1661.75 cm^{-1} in Figure 1(c) indicated the stretching vibration of carbonyl ($\gamma_{C=O}$, amide I peak).[9,10] Peaks at 1585.69 cm^{-1} in Figure 1(a), 1609.61 cm^{-1} in Figure 1(b), and 1607.80 cm^{-1} in Figure 1(c) revealed the bending vibration of the N–H bond (δ_{N-H}, amide II peak).[9,10] The strong stretching vibration of the C–N bond (γ_{C-N}, amide III peak) appeared at 1400 cm^{-1} in these membranes.[11,12] These peaks and the slight peak position shifts for the same type IR vibrations indicated that these NF-TFC membranes were made of polysulfone, sulfonated polysulfone, and different types of polyamides prepared from different diamines as showed in Figure 1.

Figure 2 was the ATR-IR spectra for the active PA layers of NF-TFC membranes prepared from different polyamines (PRP, PPD, or MPD) and TMC on PSf/SPSf alloy substrates. It was seen that the characteristic peaks of the amide group, or $\gamma_{C=O}$, δ_{N-H}, and γ_{C-N}, appeared in all the three samples. The characteristic peaks of the sulfone group, γ_s, γ_{as}, and δ_{SO_2}, and the asymmetric stretching vibration (γ_{as}) of the sulfonic acid group also appeared in these active layers, which should only appear in the whole NF-TFC membranes. These results showed that a polyamide active layer was coated on the alloy PSf/SPSf substrate and the thickness of the active layer in these samples was no more than 0.1 μm due to the depth limit of ATR-IR from the surface of the organic film (0.1 μm) according to the experiment conditions.[6] However, the peak of $\gamma_{C=O}$ at 1670.46 cm^{-1} in the PRP/TMC bulk membrane [Fig. 1(a)] shifted to 1630.61 cm^{-1} in the active layer [Fig. 2(a)]; as did the peak at 1670.46 cm^{-1} in MPD/TMC bulk membrane [Fig. 1(b)] to 1664.46 cm^{-1} in the active layer [Fig. 2(b)], respectively. The peak at 1742.09 cm^{-1} in the PPD/TMC bulk membrane disap-

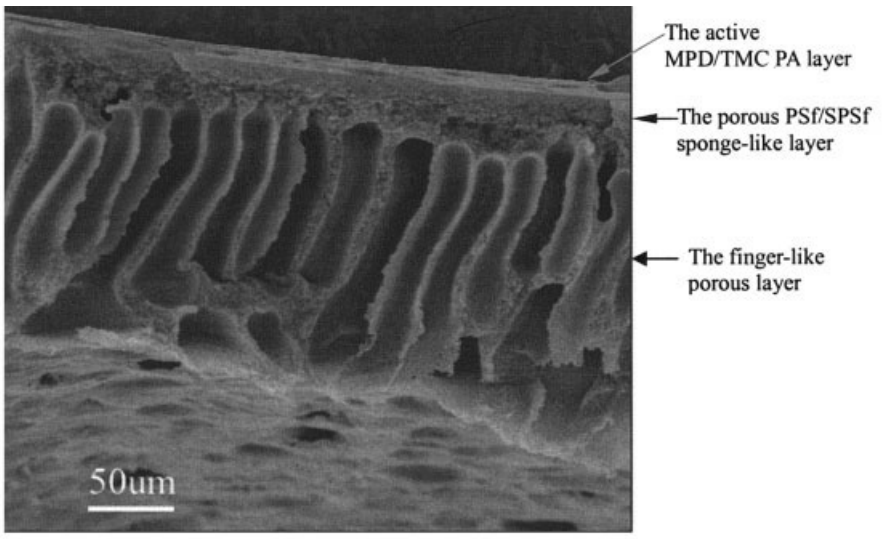

(a) NF-TFC membrane from MPD and TMC on PSf/SPSf substrate

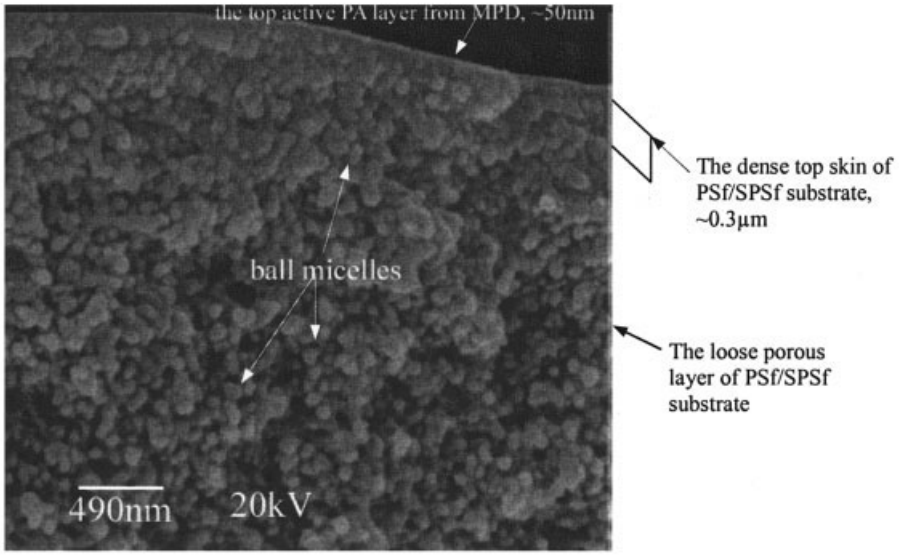

(b) Top section of NF-TFC membrane from MPD and TMC on PSf/SPSf substrate

Figure 6 SEM images of cross section structures of the NF-TFC membrane on SPSf/PSf alloy substrate: (a) the cross section of the whole membrane prepared from MPD and TMC; (b) the top active polyamide layer prepared from MPD and TMC and the porous medium layer of the PSf/SPSf substrate with ball micelles; (c) the cross section of the whole membrane prepared from PPD and TMC; (d) the top active polyamide layer prepared from PPD and TMC and the porous medium layer of the PSf/SPSf substrate with ball micelles.

peared in the active layer [Fig. 2(c)]. Peaks at 1900 cm^{-1} and 2080–2100 cm^{-1} in the bulk membranes that also appeared in the standard IR spectrum of PSf [9,10] were not present in all of the three active layers. These differences on the peaks and the peak positions for the same vibration among the top surfaces of the active layers, the bulk NF-TFC membranes, and the standard PSf substrate suggested that an interpenetrating layer might be formed between the active layers and the porous substrates.

The cross section SEM image for the NF-TFC membrane with a significant thick active layer in Figure 3(a) prepared from PPD and TMC on a PSf/SPSf substrate not only showed a valley and ridge structural active layer but also an embedded structure (see the different gray level) between the bright active layer and the dark top dense skin in the PSf/PSf porous substrate, revealing a unique layer different from the active layer and the porous substrate, while the cross section SEM image for the NF-TFC mem-

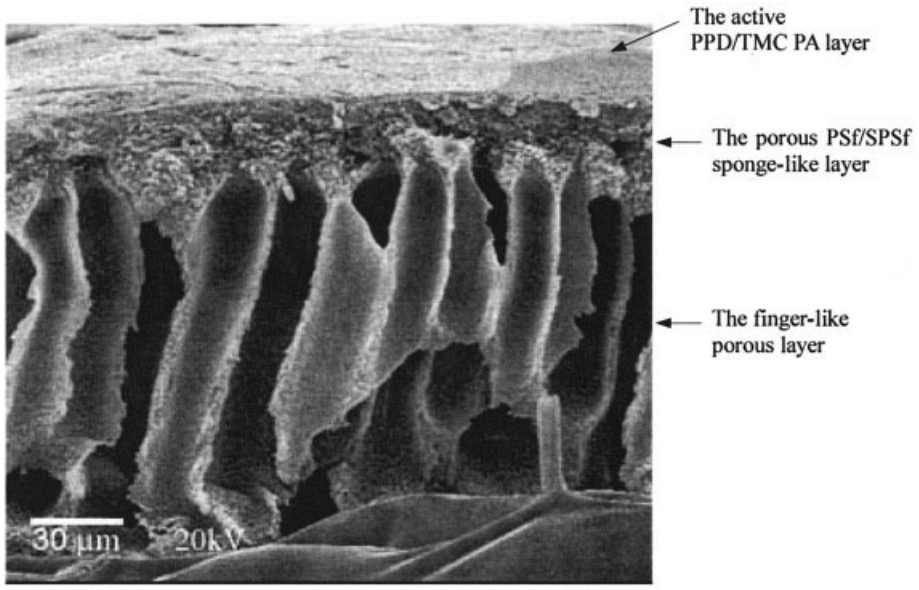

(c) NF-TFC membrane from PPD and TMC on PSf/SPSf substrate

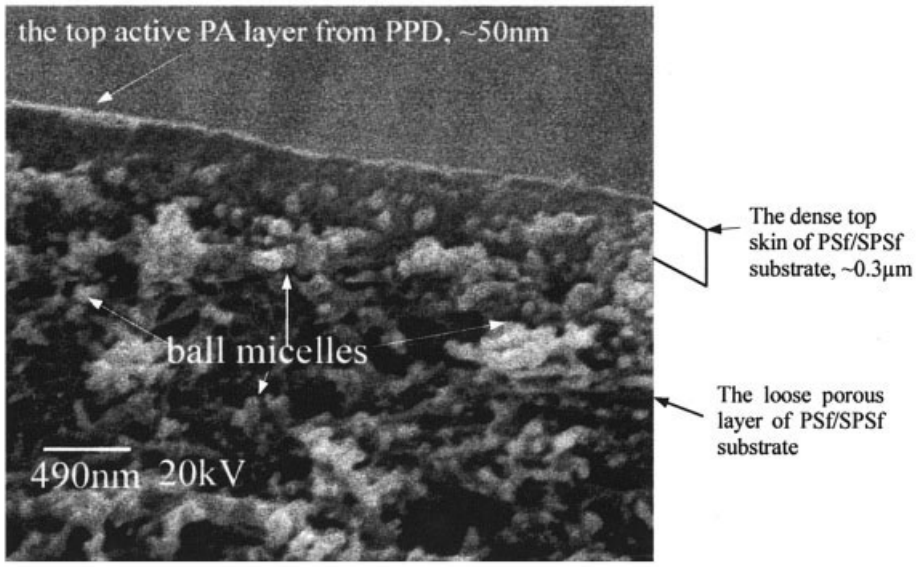

(d) Top section of NF-TFC membrane from PPD and TMC on PSf/SPSf substrate

Figure 6 (*Continued from the previous page*)

brane prepared from PRP and TMC [Fig. 3(b)] showed a flat laminar active layer on the substrates. These two figures suggested a valley and ridge structure unique in the aromatic polyamide NF-TFC membrane.

DSC analyses (Fig. 4) for the membrane with the thick PPD/TMC active layer on PSF/SPSf substrate [Fig. 3(a)], the PSf/SPSf substrate, and the PSf substrate were done for further detection of the interpenetrating layer. Distinguished from the PSf substrate and the PSf/SPSf substrate, the DSC spectrum for the NF-TFC membrane with a thick PPD/TMC active layer not only showed the crystallization temperature (T_c) of polyacrylamide at 618 K and the melting temperature range (T_m) of polyacrylamide at 655–674 K, which was similar to the standard Kevlar resin,[13] but also three different transition temperatures (T_g) and the different DSC curve shapes. The glass transition at 515 K indicated the PSf part in the NF-TFC membrane (Fig. 4, No. 2) that was similar to the T_g in the PSf/SPSf alloy substrate (Fig. 4, No. 3) but higher than the T_g of

PSf at 465 K (Fig. 4, No. 4) due to the interaction among PSf, SPSf, and polyacrylamide in the membranes. The glass transition at 575 K indicating the SPSf part in the NF-TFC membrane (Fig. 4, No. 2) was higher than that at 565 K in the PSf/SPSf substrate (Fig. 4, No. 3) due to the interaction between SPSf and polyacrylamide. The glass transitions for SPSf in the membranes were similar to the glass transition of SPSf with 65–70 mol % sodium sulfonate.[14] The transition at 593 K between the T_g of the SPSf and the T_c of the PA layer, clearly revealed a layer different from the SPSf and the active polyamide layer, which most probably represented the embedded structure layer shown in the cross section SEM image of this NF-TFC membrane. This interpenetrating layer mainly consisted of polyamide with small amount of PSf and SPSf since the transition temperature was higher than 583 K (the reported highest glass transition of SPSf).[14,15] These transitions were not possible from the degradation of these polymers since the lowest degradation temperature among PSf (see T_d in Fig. 4, No. 1), SPSf,[14] and polyacrylamide (Kevlar resin)[16] was no lower than 753 K.

There is no doubt that introduction of SPSf in PSf substrate can improve the hydrophilic property. The asymmetric membrane structure can also be modified. High asymmetric porous substrates for NF-TFC membranes were prepared conveniently by introducing SPSf into PSf substrates. Compared with the sponge-like porous PSf substrate [Fig. 5(a)] with a thick dense top skin (~ 2 μm) and a medium porous layer made of polymer nets [Fig. 5 (b)] prepared by the same process, a finger-like porous PSf/SPSf substrate [Fig. 6(a) and (c)] with a thin dense top skin (~ 0.4 μm) and a porous medium made of ball micelles was formed by introducing SPSf in PSf substrate. This difference implied that the membrane formed from SPSf/PSf preferred the nuclei and growth mechanism to form a thin dense top layer while membrane formed from the pure PSf obeyed the spiral phase separation mechanism to form a thick dense top layer.[17] On the PSf/SPSf porous substrates with higher asymmetric structure, the typical NF-TFC membrane of higher permeability with an ultrathin active PA layer (~ 50 nm thick) was prepared [Fig. 5(b) and (d)] via interfacial polymerization from different diamines and trimesoyl chloride. To 2.0 g/L $MgSO_4$ solution, the permeability can increase from 8.0 to 13.2 L m^{-2}·h^{-1} with 95% selectivity for membranes prepared from PRP, and from 4.0 to 6.1 L m^{-2}·h^{-1} with 95% selectivity for membranes prepared from MPD, and 2.8 to 4.0 L m^{-2}·h^{-1} with 98% selectivity for NF-TFC membranes prepared from PPD, by the substitution of a PSf substrate with a PSf/PSf alloy substrate. It was also found that there were no bubbles in the active layer for NF-TFC membranes on PSf/SPSf substrates after they were immersed in water for several days. However, bubbles appeared very often in the active layer for NF-TFC membranes on PSf substrates, especially for membranes prepared from PRP. These bubbles were defects in the active layers, indicating the debinding between the substrate and the active layer, which would deteriorate the selectivity of membranes during operation. The improvement of the binding between the substrate and the active layer by introducing SPSf into the substrate was probably from good compatibility obtained between the hydrophilic PSf/SPSf substrate and the polyamide active layer.

Different from the NF-TFC membrane with a thick active layer, these NF-TFC membranes with a thin active layer did not show a ridge and valley structure but a flat laminar structure in the active layer even for membranes prepared from polyacryamide [Fig. 6 (b) and (d)], similar to that of the PRP/TMC NF-TFC membrane in Figure 2(b). These results suggested that the ridge and valley structure might develop from the growth of the stiff aromatic polyamide chains perpendicularly to the interface between the aqueous phase and the organic phase, which conformed to the membrane growth mechanism advanced by Enkelmann and Wegner.[18] While only the active layers grew up to a certain thickness, the ridge and valley structure be-

TABLE I
Membrane Separation Performance for Different Salt Solutions

Membranes		NaCl solution		$CaCl_2$ solution	$MgSO_4$ solution	$FeCl_3$ solution
		0.5 g · L^{-1}	2.0 g · L^{-1}	0.5 g · L^{-1}	2.0 g · L^{-1}	1.0 g · L^{-1}
PRP/TMC	F (L · m^{-2} · h^{-1})	8–13	7–10	—	5–20	8–10
	R (%)	35–50	30–39	—	85–95	75–81
PPD/TMC	F (L · m^{-2} · h^{-1})	3–5	4–6	4–6	2–5	—
	R (%)	80–97	70–75	90–93	92–99	—
MPD/TMC	F (L · m^{-2} · h^{-1})	—	—	—	5–7	—
	R (%)	—	—	—	95–97	—

TABLE II
Ground Water Softening Results Using Two Kinds of NF-TFC Membranes

Membranes	F ($L \cdot m^{-2} \cdot h^{-1}$)	λ_f ($m\Omega^{-1} \cdot cm^{-1}$)	λ_P ($m\Omega^{-1} \cdot cm^{-1}$)	R (%)
PRP/TMC	13.2	1.25	0.2	84.0
PPD/TMC	4.2	1.25	0.1	92.4

came significant to be observed for active layers prepared from polyacrylamide with stiff chains.

Membrane application

The results for the separation of different valence salts in Table I showed that these membranes had higher selectivity with reasonable flux rates for polyvalent ions than for monovalent ions under ultralow pressure drop (0.3 MPa). Both salts with polyanions (i.e., SO_4^{2-}) and salts with polycations (i.e., Fe^{3+}) showed a higher selectivity due to the charged surface of these membranes[1,5] and their huge effective aqua-ion radius from high valence. Both the selectivity and the flux rate decreased when the concentration of the salt solution increased, which resulted from the higher ion strength and the higher osmosis pressure at higher salt concentration. PPD/TMC and MPD/TMC membranes had higher selectivity and lower permeability than PRP/TMC membranes, which indicated that aromatic diamines facilitated the formation of a denser active layer due to their stiff molecular chains than did alicyclic diamines.

Table II shows the results of softening the ground water in Beijing. PRP/TMC membranes had a higher flux rate while PPD/TMC membranes had a higher rejection rate. There was no white or colorful precipitate (colorful materials were from the heavy metal ion and some organics) settling down in the boiling water if the water was purified using these membranes while much white or colorful precipitate appeared in the boiling water if water was not treated.

PRP/TMC membranes and PPD/TMC membranes were also used to purify two kinds of wastewater from the adipic acid plant of Yueyang Petroleum Chemical Inc. of China. One was from the catalyst workshop, which included high concentrations of ammonia salts and other nitrides with pH 2–3, called H-NH_4^+/N wastewater. The other was the combined sewage with pH 7.5, called T-W wastewater. Table III shows that the two kinds of membranes had reasonable fluxes and rejection rates under 0.3 MPa. The pH of H-NH_4^+/N increased from 2–3 to 4–5 and that of T-W wastewater was reduced from 7–8 to 5–6 after treatment. The general salt content in the wastewater was reduced by three to five times using these membranes. These membranes could be used in acidic environments with pH values of 2–3. PPD/TMC membranes still had the higher salt rejection rate and PRP/TMC had the higher flux rate. If several treatment processes using these NF-TFC membranes were sequenced together, better results would be obtained.

CONCLUSIONS

The NF-TFC membranes of excellent separation performance were prepared via interfacial polymerization from three kinds of diamines and trimesoy chloride on PSf/SPSf alloy substrates. The thickness of the thin active polyamide layer ranged from no more than 50 nm to several microns. A ridge and valley structure was formed in the thick active polyamide layer of the NF-TFC membrane prepared from aromatic monomers. Investigation of the chemical composition, the cross section structure, and the thermal property of NF-TFC membrane revealed an interpenetrating layer between the active layer and the substrate. Introduction of SPSf into the PSf porous substrates not only improved the hydrophilic property of membranes and the binding between the active PA layer and the substrate, but also modified the asymmetric membrane structure, which endowed the NF-TFC membrane on the PSf/SPSf substrate with a higher permeability than those on the PSf substrate. These kinds of NF-TFC membranes could be used in separating polyvalent ions, softening underground water, and purifying wastewater under

TABLE III
Treatment of Two Types of Sewage from the Adipic Acid Plant Using Two Types of NF-TFC Membranes

Wastewater type	Membrane type	λ_f ($m\Omega^{-1} \cdot cm^{-1}$)	λ_P ($m\Omega^{-1} \cdot cm^{-1}$)	R (%)	F ($L \cdot m^{-2} \cdot h^{-1}$)
H-NH_4^+/N	PRP/TMC	12.8	4.3	66.4	2.3
	PPD/TMC	12.8	2.6	79.0	0.8
T-W	PRP/TMC	7.5	2.0	73.3	2.5
	PPD/TMC	7.5	1.5	80.0	0.9

ultralow pressure at a wide pH range. To the groundwater with primary conductivity of 1.25 $m\Omega^{-1} \cdot cm^{-1}$, the net desalination rate reached 84–93% with fluxes of 3.2–13.2 $L \cdot m^{-2} \cdot h^{-1}$. For wastewater containing nitrides and ammonium salts from apidic acid plants, the conductivity of wastewater could be reduced by three to five times with fluxes of 0.8–2.5 $L \cdot m^{-2} \cdot h^{-1}$.

The support of this work by NL Chemical Ltd. is gratefully acknowledged. The authors thank Prof. Quan Zhang for SEM images, Dr. Fang Wang for FT-IR and ATR spectra, and Prof. Youqing Hua for DSC spectra.

References

1. Petersen, R. J. J Membr Sci 1993, 83, 81.
2. Song, Y.; Zhao, C.; Liu, F.; Yang, Y.; Tian, D.; Zhong, T.; Sun, B. Huagong Keji (Sci Technol Chem Ind China) 1999, 7, 1.
3. Song, Y.; Liu, F.; Zhao, C.; Sun, B. J Beijing Univ Chem Technol 1999, 26, 38.
4. Song, Y.; Liu, F.; Sun, B. Fangzhi Kexue Yanjiu (Textile Sci Res) 1999, 10, 13.
5. Porter, M. C. In Handbook of Industrial Membrane Technology, Thin Film Composite Reverse Osmosis Membranes; Noyes Publications: Park Ridge, NJ, 1995; Chap 5, pp. 308, 328.
6. Song, Y.; Liu, F.; Yang, R.; Zhao, C.; Sun, B. J Tianjin Inst Textile Sci Technol 1999, 18, 102.
7. Sourirajan, S. Mo Fenli Kexue Yu Jishu (Membr Sep Sci Technol) 1984, 4, 88.
8. Morgan, P. W. Condensation Polymers by Interface and Solution Methods; Interscience: New York, 1965.
9. Jing, X.; Chen, S.; Yao, E. Application Direction of Infrared Spectrum; Tianjin Science and Technology Publisher: Tianjin, 1992; 1st ed, Chap 18, pp. 25, 33–36.
10. Xie, J. Application of Infrared Spectrum on the Organics and Pharmacy Chemistry; Science Publisher: Beijing, 1987; 1st ed, Chap 15.
11. Zhang, S.; Ying, D. Infrared Spectrum Analysis and New Technology; China Pharmacy Technology Publisher: Beijing, 1993; 1st ed.
12. Monomers and Polymers IR Grading Spectra; Sadtler Research Laboratories Inc: Philadelphia, PA, 1971; Vols. 10–12, pp. 13–15, 19–21.
13. Jin, R .; Hua, Y. In Polymer Physics; Chemical Industry Publisher: Beijing, 1990; p. 98.
14. O'Gara, J. F.; Williams, D. J.; Macknight, W. J. Karasz, F. E. J Polym Sci, Part B: Polym Phys 1987, 25, 1519.
15. Noshay, A.; Robeson, L. M. J Appl Polym Sci 1976, 20, 1885.
16. Pektas, I. J Appl Polym Sci 1998, 67, 1877.
17. Olabisi, O.; Robeson, L. M.; Shaw, M. T. Polymer–Polymer Miscibility; Academic Press: New York, 1979.
18. Enkelmann, V.; Wegner, G. Makromol Chem 1976, 177, 3177.